Dendrite-Tolerant All-Solid-State Sodium Batteries and An Important Mechanism of Metal Self-Diffusion

Chih-Long Tsai[#a], Tu Lan[#a,b], Christian Dellen[a], Yihan Ling[a,c], Qianli Ma*[a], Dina Fattakhova-Rohlfing[a,d], Olivier Guillon [a,e], Frank Tietz[a]

[a] *Forschungszentrum Jülich GmbH, Institute of Energy and Climate Research, Materials Synthesis and Processing (IEK-1), 52425 Jülich, Germany*
[b] *Institute of Mineral Engineering, RWTH Aachen University, 52062 Aachen, Germany*
[c] *School of Materials Science and Engineering, China University of Mining and Technology, Jiangsu Province, Xuzhou 221116, P. R. China*
[d] *Department of Engineering and Center for Nanointegration Duisburg - Essen (CENIDE), Universität Duisburg - Essen, 47057 Duisburg, Germany*
[e] *Jülich Aachen Research Alliance, JARA-Energy, 52425 Jülich, Germany*

[#] These authors contributed equally to this work
* Corresponding author
E-mail addresses: q.ma@fz-juelich.de

Keywords:
All-solid-state battery
Sodium battery
Dendrite
NaSICON
Metal Self-diffusion

ABSTRACT

Inhibition of dendrite growth in all-solid-state lithium batteries (ASSLBs) has long been a challenge to the field. In the present study, the conditions for dendrite growth for a similar but less mature technology, all-solid-state sodium batteries (ASSNBs), are investigated. By simply sticking sodium metal to $Na_{3.4}Zr_2(SiO_4)_{2.4}(PO_4)_{0.6}$ (NZSP) ceramic pellets and without applying external pressure during operation, the critical current density of Na/NZSP/Na symmetric ASSNBs reaches 9 mA cm^{-2} at 25°C. The cells can be stably operated at an areal capacity of 5 mAh cm^{-2} (per half cycle, with 1.0 mA cm^{-2}) at 25°C for 300 h in a galvanostatic cycling measurement without any dendrite formation. The results outperform the existing ASSLBs and ASSNBs, and also go beyond satisfying the requirements for practical applications. The influence of the high metal self-diffusion coefficient on the dendritic plating/stripping is regarded as the most likely reason for the high dendrite tolerance of ASSNBs. A mathematical model based on Fick's second law was applied as a first approximation to illustrate this influence. Full ASSNBs were fabricated with infiltrated $Na_3V_2(PO_4)_3$ (NVP) as the cathode and can be stably operated with a capacity of 0.60 mAh cm^{-2} at high rate of 0.5 mA cm^{-2} at room temperature.

1. Introduction

Among commercialized energy-storage systems, Li-ion batteries (LIBs) have gained worldwide acceptance in various market segments because of their high energy density, efficiency and long cycle life. They are also regarded as promising stationary energy-storage systems for fluctuating energy sources, such as solar and wind power, the future energy solutions of mankind [1]. However, it is estimated that until 2050, increment of 1×10^{17} Wh should be installed per year to satisfy the increasing energy demands [2]. To store such an amount of energy, 9×10^{9} tons of lithium metal is demanded, while the global annual Li production is only 8×10^{4} tons in 2018 [3]. Consequently, Na-ion batteries (NIBs) have attracted increasing attention in recent years because of their electrochemical similarity to LIBs, the abundant and convenient resources required to produce them, and the low price of starting materials [2, 4-7].

Besides the increasing demand of critical resources for battery production, the market requirements necessitate a significant increase in the energy density of batteries to satisfy the steadily growing electrical energy consumption. One intensively explored trend in battery research is the use of solid-state electrolytes in e.g. all-solid-state Li-batteries (ASSLBs) or all-solid-state Na-batteries (ASSNBs), which have the potential to compete the energy density of the very mature conventional LIBs [5, 7-9]. An important prerequisite for the performance breakthrough, however is the use of metallic anodes, which poses serious challenges in conventional electrolyte systems due to the reactivity with the electrolyte and the mossy dendritic growth upon multiple cycling [5-8, 10-11]. For a long time it has been believed that the solid electrolytes with high shear modulus (which is the case for the ceramic electrolytes) can mitigate dendrite formation. However, a multitude of experimental evidence from recent years confirms that lithium dendrites can propagate through the solid electrolytes resulting in

rapid cell fading. A solution to this problem (relevant for all kinds of batteries with Li-metal anodes) is still lacking and is a focal point in recent battery research [7, 9, 11]. The typical expectation for ASSLBs is an areal capacity of ≥ 3 mAh cm^{-2} (per half cycle, e.g. a plating or a stripping of Li metal electrode) at a current density of ≥ 1 mA cm^{-2} [10]. No ASSLB has been reported to date that has reached this criterion at room temperature. For the moment, less attention has been paid to this issue in the field of ASSNBs, because their development is not as advanced as ASSLBs [7, 11]. However, at this point, there seems to be no reason for different mechanisms of dendrite formation in ASSLBs and ASSNBs [12-14]. Consequently, comparison of dendrite growth in ASSLBs and ASSNBs has not been carried out yet and the evaluation of operating conditions leading to short-circuiting and battery failure.

Very recent investigations point out that the morphological conformity of the metal/solid electrolyte interface (both during metal dissolution in a discharge process and electroplating in the charging cycle), and the steady state flow of metal ions between the current collectors through the bulk battery components and the interfaces, are the key prerequisites for stable dendrite-free battery operation [7, 11, 13]. Any inhomogeneity of the interface arising during battery processing and operation (e.g. due to the different rates of metal dissolution and diffusion in grains and along grain boundaries, or the loss of contact) may result in inhomogeneous electric field and the diffusion conditions, promoting dendrite formation.

Only recently, a few studies started to contemplate the relationship between the self-diffusion of metal electrodes and dendrite formation in ASSLBs. Krauskopf et al. correlated the formation of dendrites with self-diffusion of lithium metal and identified the vacancy diffusion coefficient in lithium metal as a fundamental physico-chemical limitation of the lithium metal anode under anodic load [15]. Kasemchainan et al [16]. and Wang et al [17]. further pointed

out that the accumulated metal vacancies (generated by the mismatch of Li self-diffusion and current density) near the interface between lithium and ceramic electrolyte can be eliminated by external pressure of several MPa. Thus the dendrite tolerance of the cells can be greatly increased with permanent applied pressure during operation. However, until now the most fundamental question, i.e. the relationship between the metal self-diffusion coefficient, the current density and the areal capacity is not mathematically described for solid-state metal batteries. In addition, the practical limitations for ASSNBs have also been insufficiently addressed.

In the present study we demonstrate that the symmetric cells assembled with metallic Na as anode in combination with NaSICON-type solid electrolyte $Na_{3.4}Zr_2(SiO_4)_{2.4}(PO_4)_{0.6}$ (NZSP, showing high bulk and a total conductivity of 1.5×10^{-2} S cm^{-1} and 5×10^{-3} S cm^{-1}, respectively [18]) can stably operate at high current densities and high metal loads outmatching the existing ASSLBs and ASSNBs, and even the state-of-the-art batteries with liquid or polymer electrolytes. In addition, a mathematical model is established to describe the relationship between the metal self-diffusion coefficient, the current density and the areal capacity. The high dendrite tolerance of ASSNBs is accordingly attributed primarily to the high self-diffusion coefficient of sodium.

.

2. Experimental Section

2.1. Fabrication and characterization of powders and symmetric cells

NZSP powder was synthesized on a laboratory scale (10 g – 1 kg per batch) using a solution-assisted solid-state reaction method (SA-SSR). $NaNO_3$ (VWR), $ZrO(NO_3)_2$ (Aldrich), $Si(OCH_2CH_3)_4$ (Merck), and $NH_4H_2PO_4$ (Merck) were used as starting materials. All the

chemicals applied in this study are analytically pure. Stoichiometric amounts of $NaNO_3$ and $ZrO(NO_3)_2$ were dissolved into deionized water. A stoichiometric amount of $Si(OCH_2CH_3)_4$ was also added to the solution while stirring. When $Si(OCH_2CH_3)_4$ was hydrolyzed, the stoichiometric amount of $NH_4H_2PO_4$ was added to the system during stirring. The homogeneous aqueous solution immediately showed formation of complex zirconium oxyphosphate compounds. The whole mixture was dried at 85 °C. The dried powder was calcined at 800 °C for 3 h. After calcination, a white powder was obtained. The calcined powder was then milled in ethanol with zirconia balls on a milling bench for 48 h, and dried at 70 °C for 12 h. Details of the synthesis can be found in our previous publications [18-19].

NZSP powder was put into a cylindrical pressing mold with the diameter of 13 mm and pressed with a uniaxial pressure of 100 MPa at room temperature. The green density of the as-pressed pellet is about 50 % of the theoretical density of NZSP (the theoretical density of NZSP is 3.29 g cm^{-3}).The pressed pellets were sintered at 1260 °C for 5 h. The obtained pellets had a diameter of about 10 mm and a thickness of 1-2 mm (corresponding to about 20 % shrinkage of both the diameter and thickness after sintering). The relative density of the sintered pellets was >95 %. The detailed crystallographic analysis of NZSP can be found in [18].

Na-metal sheets were attached to NZSP pellets by mechanical pressing with the force of about 1 kN (~12 MPa). The thickness of the Na-metal electrode is 0.5 – 1 mm. All electrochemical tests of the Na/NZSP/Na symmetric cells were carried out inside Swagelok cells. No extra pressure was applied during cell testing. The impedance spectra of the Na/NZSP/Na symmetric cells were measured at 25 °C using a commercial electrochemical system (Biologic VMP-300), with an AC frequency range from 3 MHz to 1 Hz, and fitted with the software “Z-view” (Scribner Associates Inc.). The current-voltage behavior of the cells was tested using an electrochemical system (Biologic VMP-300) with controlled temperature in a climate chamber (Vötsch, VT4002).

2.2. Fabrication and characterization of full cells

Part of the NZSP powder was mixed with 10 wt. % rice starch. The mixture and pure NZSP powder were put into a cylindrical pressing mold (diameter 13 mm) layer by layer, and then pressed. The pressed pellets were sintered in air at 1280 °C for 6 h to produce the dense-porous bi-layered NZSP pellets.

NVP precursor solution was made by mixing ethanolamine (Merck), citric acid (Merck), de-ionized H_2O, NaH_2PO_4 (Sigma-Aldrich) and NH_4VO_3 (Merck). The solution was deposited onto the surface of the porous layer for infiltration and propagated by capillary forces.

The pellets were then heat treated at 740 °C in Ar-4 %H_2 for 4 h to form the NVP crystalline phase. The infiltration and heating process was repeated several times to obtain the desired loading of active material and establish continuous electronic pathways. Na metal sheets were then stuck to the prepared half cells to finish the fabrication of the full cells. The cells were sealed in Swagelok cells after assembling. More fabrication details can be found in the former publication [20]. The charge-discharge behaviors of the batteries were measured using an electrochemical testing system (Biologic VMP-300) at the constant temperature of 25 °C in a climate chamber (Vötsch, VT4002).

3. Results and discussion

3.1 Electrochemical behaviors of symmetric SSNBs

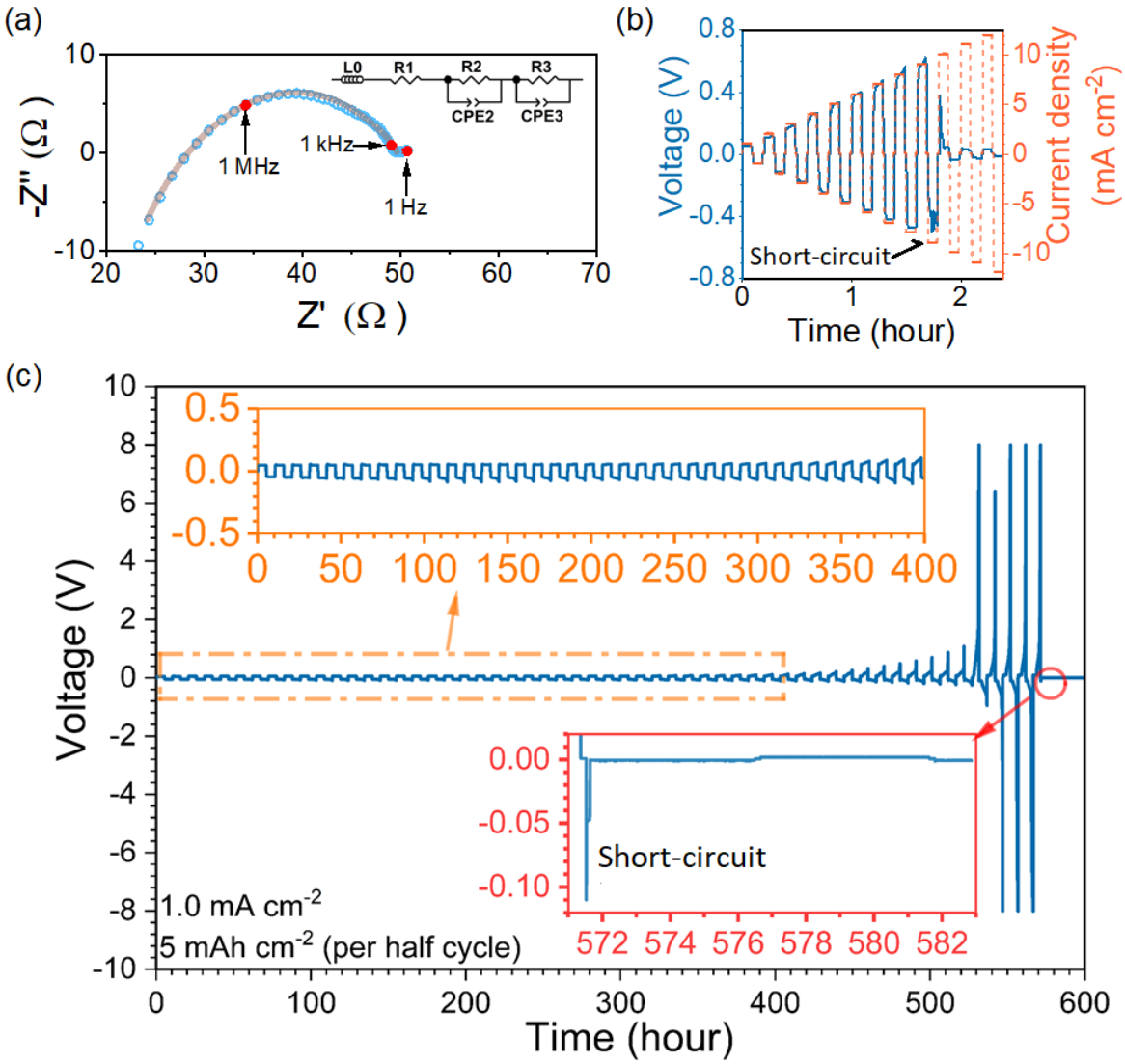

Figure 1. a) Experimental Nyquist plot (blue circles) of the impedance spectrum recorded at 25 °C for a Na/NZSP/Na symmetric ASSNB (NZSP with diameter of 10.3 mm and thickness of 1.8 mm), together with the simulated data (solid line). The equivalent circuit used for the data simulation is shown in the inset, where L0, R and CPE indicate the inductance induced by conductive parts in the measurement setup, resistance and constant phase elements, respectively. b) DC cycling of a Na/NZSP/Na symmetric ASSNB, incrementally increasing the current density from 1.0 to 9.0 mA cm^{-2} (5 min per half step). The blue line indicates the change in voltage and the orange dash indicates the change in current density. c) Galvanostatic cycling of a Na/NZSP/Na symmetric ASSNB at 1.0 mA cm^{-2}, 5 mAh cm^{-2} (per half cycle) and 25 °C. Partially enlarged plots are also shown as inlets. No pressure was applied during all the tests in **Figure 1**.

Table 1: Parameters of the equivalent circuit shown in **Figure 1**a.

Lo (H)	R1 (Ω)	R2 (Ω)	Capacitance of CPE2 (F)	R3 (Ω)	Capacitance of CPE3(F)
1.1×10^{-6}	10.4	35.3	2.4×10^{-9}	4.0	3.6×10^{-7}

During the operation or testing of all the cells in this work, no external pressure was applied. The resistance of a typical Na/NZSP/Na symmetric cell was investigated by impedance spectroscopy. **Figure 1**a shows the Nyquist plot of the cell at 25 °C, together with the fitted data and the corresponding equivalent circuit used for the data, where L0, R and CPE indicate the inductance, resistance and constant phase element (CPE), respectively. The relative parameters of the equivalent circuit are shown in **Table 1**. R1 and R2 are typically attributed to the bulk and grain-boundary resistance of NZSP, respectively [18-19]. Although the high-frequency semi-circle representing the bulk behavior R1 is only visible as the left intercept with the x-axis in the obtained spectrum, the sum of R1 and R2 can be assigned as the total resistance for the measured NZSP, which is 45.7 Ω. Together with the dimension of the sample (a diameter of 10.3 mm and a thickness of 1.8 mm), the total ionic conductivity of the sample, σ, can be calculated by the following equation:

$$\sigma = \frac{l}{(R1+R2)A} \quad (1)$$

where l is the thickness of the sample), and A is the electrode area of the sample pellet. The value of σ is 4.7×10^{-3} S cm^{-1}, which matches well with the previously reported conductivity of NZSP [18]. R3 can then be assigned to an interface resistance between Na and NSZP, which is 4.0 Ω and corresponds to 1.7 Ω cm^2 (for each interface of Na/NZSP). It should be noted that the interface resistance between Na metal and solid state electrolyte was reported to be in the range of hundreds of Ω cm^2 [12, 19]. Only in our earlier work a similar contact resistance of 4.1 Ω cm^2 has been shown [18]. It should be emphasized that such low interface resistance

between Na and NSZP is achieved from the as-sintered surface of pristine NZSP. When NZSP samples were polished by sandpaper, interface resistance between Na and NSZP is much larger. The details are shown in the Supporting Information **Figure S**1. The high ionic conductivity of NSZP might be one of the reasons for the favorable interface resistance. Ideal interface compatibility between Na-metal and NZSP ceramic is also expected to be important for the low interface resistance. However, further advanced characterization of the interface behavior is necessary to explain the point (the surface morphology of NZSP is shown in the Supporting Information **Figure S**2). In comparison, the best reported interface resistance between Li-metal and the solid-state electrolyte is 2Ω cm^2.[14] However, complicated heat-treatment was applied to establish contact between the Li-metal and the electrolyte, while in the present study, Na-metal is stuck to NZSP ceramic simply by applying mechanical load, which is released during operation.

The critical current density (CCD) of a symmetric ASSNB cell was characterized by DC cycling analysis at 25 °C, where CCD is defined as the lowest current density at which cell short-circuiting occurs due to metal penetration. Typical CCD behavior of the Na/NZSP/Na symmetric ASSNB is shown in **Figure 1**b. The initial total resistance of the symmetric cell is 63 Ω. A short circuit happens at -9 mA cm^{-2}, indicating dendrite formation. In the present study, the CCDs over the same step-time (5 min per half cycle) range from 5 to 9 mA cm^{-2}. It should be emphasized that in addition to the current density, the step time is also an important parameter for the CCD measurements. When a longer step time is applied, the CCD values decrease. 15 and 30 min step-times (per half cycle) result in CCD ranges from 3 to 6 and from 2.5 to 3.5 mA cm^{-2} (Supporting Information **Figure S**3), respectively. Nevertheless, the values are higher than the best reported result of Li-counterparts (~0.9 mA cm^{-2} at room temperature, when a 15 min step-time is applied [14]).

Table 2. Performances of different Na / NaSICON / Na based symmetric cells

Composition of NaSICON	Interface resistance (Ω cm²)	Current density (mA cm⁻²)	Areal capacity per half cycle (mAh cm⁻²)	Operating time (h)	Temperature (°C)	Ref.
$Na_{3.1}Zr_{1.95}Mg_{0.05}(SiO_4)_2(PO_4)$	---	0.044	0.09	4.7	25	[21]
$Na_3Zr_2(SiO_4)_2(PO_4)$	---	0.2	0.1	70	RT	[22]
$Na_3Zr_2(SiO_4)_2(PO_4)$	400	0.15 – 0.25	0.15 – 0.25	550	65	[12]
$Na_{3.2}Zr_{1.9}Ca_{0.1}(SiO_4)_2(PO_4)$	175	0.1 – 0.3	0.1 – 0.3	600	RT	[23]
$Na_{3.4}Zr_2(SiO_4)_{2.4}(PO_4)_{0.6}$	4	0.6	1.8	180	RT	[18]
$Na_3Zr_2(SiO_4)_2(PO_4)$ deposited with Graphene	46	1	1	1000	RT	[24]
		2	2	50		
$Na_{3.4}Zr_2(SiO_4)_{2.4}(PO_4)_{0.6}$	1.7	0.5	2	313	0	This study
		1.0	5	571	25	

Typical galvanostatic cycling behavior of a Na/NZSP/Na symmetric ASSNB (initial total resistance: 49 Ω) operating at 25 °C is shown in **Figure 1**c, where ±1.0 mA cm^{-2} is applied to the cell for 5h per half cycle, i.e. areal capacity of 5 mAh cm^{-2}. The plateau voltage for the cycling is 46 mV at the beginning. The cell behaves stably at the first 300 h, with plateau voltage remaining at about 50 mV. After 300 h, slight polarization starts to be observed from the plot by the increasing voltage. At 400 h, the plateau voltage during is increased to maximally 100 mV during charging or discharging. After 400 h, the polarization becomes severe, which shows maximal voltage of 0.7 V at 500 h, and as high as 8 V at 530 h. It is generally agreed that such polarization between metal electrode and solid-state electrolyte is because of the resistance increase of symmetric cells caused by the continuous contact-loss between the electrode and electrolyte during operation. Under critical condition the contact-loss leads to point-contact and dendrite is then formed because of the extremely high local current at the position of the point-

contact [7, 11, 13, 15-17]. In this explanation, when the plateau voltage is 8 V in the present study, the local current density should be as high as 174 mA cm^{-2} (although only for very short time), considering the plateau voltage is 46 mV at the beginning, and Na and NZSP is assumed to be fully contacted at the time. Under such extreme condition, the symmetric cell still persevered for four and half cycles. At 571 h, short-circuit happens and plateau voltage decreases to only 1 mV. Even at 0 °C, a Na/NZSP/Na symmetric ASSNB can still endure ±0.5mA cm^{-2} and 2 mAh cm^{-2} per half cycle (Supporting Information **Figure S**4), operating more than 300 h without any dendrite formation. **Table 2** compared the performances of the present Na / NaSICON / Na symmetric cell and published results, indicating the dominance of this study. As for lithium based cells, Albertus et al. [10] reviewed 26 top-performance lithium batteries with different kinds of electrolytes (solid-state, liquid or polymer). Among them only one cell based on liquid-containing polymer electrolyte shows a higher areal capacity (6 mAh cm^{-2} per half cycle at ±3 mA cm^{-2}, room temperature [25]) than the one in this study. If only ASSLBs are considered and similar testing conditions are applied (i.e. pure Li sheets, no three-dimensional ceramic-metal structures were applied as negative electrodes [26], and no extra pressure applied during testing [16-17]), the best ever reported symmetric ASSLB was operated at ±1.0 mA cm^{-2} and 3 mAh cm^{-2} per half cycle, but at a higher temperature of 60 °C [27]. At room temperature, areal capacity of only 0.2 mAh cm^{-2} per half cycle at ±0.2 mA cm^{-2} could be reached for symmetric ASSLBs [14].

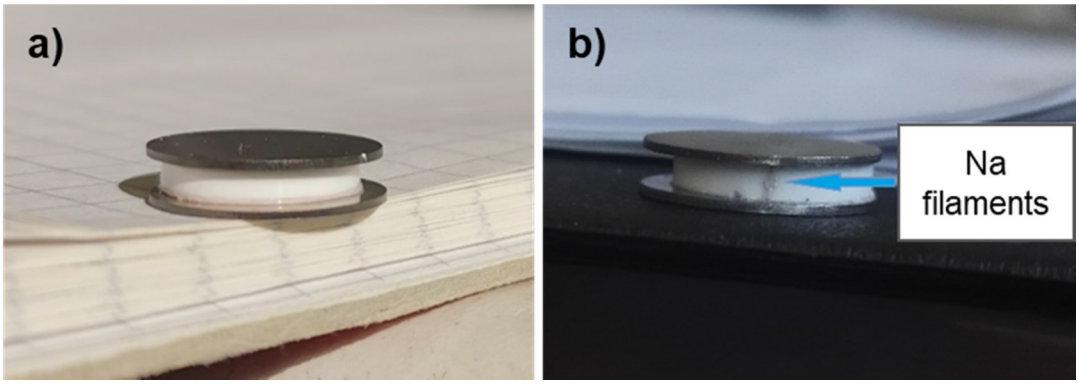

Figure 2. Photograph of typical Na/NZSP/Na symmetric cells: a) as prepared, and b) with sodium filament grown across on the side of the electrolyte pellet after CCD measurement as described in **Figure S3b**. Ni pellets have been used on both sides as current collectors.

The typical appearance of Na/NZSP/Na symmetric cells before and after cycling is shown in **Figure 2**. Unlike the ASSLBs cells with Li metal anodes, in which Li dendrites grow through the ceramic electrolyte [7, 11, 13, 15-17], the Na metal creeps to the sides of the ceramic pellets and forms bridge contacts (filaments) between both Na electrodes (**Figure 2b**) that short circuit the cell. This behavior was observed for all short-circuited samples tested in this work. The absence of the dendritic growth through the ceramics is supported also by the fact that no dark areas are observed in the NZSP electrolyte of short circuited cells. When a metal dendrite forms and grows into the ceramic electrolyte, dark spots are usually found at the position of the dendrites [28]. However, after removing the Na metal (with water) from the samples, the exposed surface of the NZSP pellets of short circuited cells remains practically unchanged (see **Figure S2** in the Supporting information).

Based on the provided experimental evidence it can be asserted that the mechanism of short circuiting in NZSP-based ceramic cells with Na electrodes is different from that observed in the solid state cells with Li metal electrodes. Although the mechanism of this phenomenon is not investigated yet, it is possible that the more ductile sodium and faster surface diffusion of Na as compared to Li prevent the dendrite formation and are responsible for this effect.

It should be mentioned that although the solid electrolyte/metal interface is very important for stable battery operation, it is not the only factor responsible for dendrite formation. For example, the interface resistance of the ASSLBs in Ref. 14 is similar to the present study (2 Ω cm^2 *vs*. 1.7 Ω cm^2, respectively, both at room temperature), but the CCDs for dendrite formation are very different (0.9mA cm^{-2} *vs*. 9 mA cm^{-2} in this study), and so are the galvanostatic cycling performances (0.2 mAh cm^{-2} *vs*. 5 mAh cm^{-2} in this study). Apparently, besides the difference in the surface conditions of different solid-state electrolyte applied in the batteries, further mechanisms influencing the metal-plating/stripping behavior must exist.

3.2 The influence of metal self-diffusion

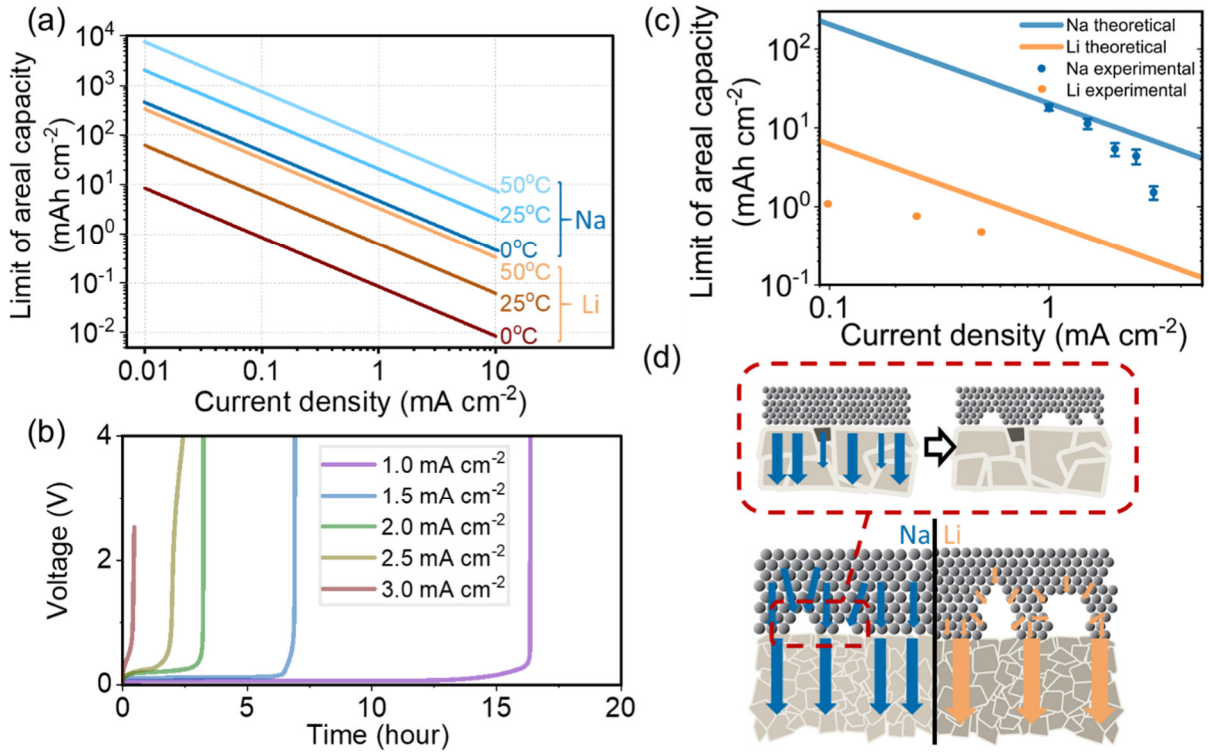

Figure 3. a) Calculated $C_{A\,lim}$ as a function of current density at different temperatures for ASSLBs and ASSNBs. b) DC polarization experiments (at 25°C) on Na/NZSP/Na symmetric cells. c) Tested limit of areal capacity at 25°C as a function of current density for SSNBs in comparison to calculated values for ASSNBs and ASSLBs. d) Schematic explanation of practical DC polarization behavior for ASSNBs (ASSLBs).

During the galvanostatic cycling of SSBs with metal anodes, the transfer of metal ions into the solid electrolyte is motivated by electromotive force (which appears as current), while the replenishment of metal atoms in the metal is motivated by the self-diffusion. At the interface between the metal and ceramic, the flux of ions through the interface and the self-diffusion may have a mismatch, which might be the origin of the dendrite formation. Very recently, several groups started to perceive the relationship between metal self-diffusion and dendrite formation [15-17]. In the present study, the mechanism is explained by a mathematical model. The half-cell reaction in the anode part of a SSB with metal anode involves three processes: (i) charger transfer processes at the interface (oxidation of metal atoms to form ions during discharging, or reduction of metal ions to atoms during charging), and two bulk transport processes: (ii) the transport of generated metal ion into the solid electrolyte and the formation of local vacancies at the metal/solid electrolyte interface, and (iii) the diffusion of metal atoms in the bulk of the metal anode towards the interface. The similar rates of the different processes (steady state condition) define the stability of the battery operation. Process (iii) can be expressed by Fick's second law:

$$\frac{d\varphi}{dt} = D\,\frac{d^2\varphi}{dx^2} \tag{2}$$

where φ is the concentration of metal atoms in the anode, t is time, D is the self-diffusion coefficient of metal atoms in the metal and x is the distance between a metal atom and the metal/solid electrolyte interface. The following assumptions are also set as the preconditions of the model: 1) a constant current density I_D is applied to the cell, 2) the surface of a solid

electrolyte is fixed in all dimensions because the ceramic electrolyte is assumed to be a rigid body, 3) the surfaces of both metal and solid electrolytes have no defects and the contact is also perfect, 4) no extra pressure is applied on the metal and 5) the thickness of the Na electrode is much larger than the amount of Na transfer through the electrolyte during operation.

The above is solved as to **Equation** (3), which is also known as Cottrell's Equation [29]. The detailed solving steps are shown in the Supporting Information **Equation** (S1)-(S7).

$$I_D = \frac{1}{2}\varphi F(\pi D)^{0.5} t_{max}^{-0.5} \quad (3)$$

where F is the Faraday constant. According to this model, the I_D through the cell cannot stay constant for an infinite length of time because of the limit of the diffusion. The detachment of the Na electrode will finally happen when the operation exceeds a critical time, $tmax$. Furthermore, since

$$C_A = I_D \times t \quad (4)$$

where C_A (mAh cm^{-2}) is the areal capacity of the cell, and t (h) is the operating time, it can be concluded that

$$C_{A\,lim} = \frac{1}{4}\pi\varphi^2 F^2 D (I_D)^{-1} \quad (5)$$

by combining **Equation** (3) and (4), where $C_{A\,lim}$ is the theoretical limit of C_A under the particular I_D.

The self-diffusion coefficient D is the intrinsic property of a certain metal, and is a function of temperature. The temperature dependence of the self-diffusion coefficient for Li and Na (D_{Li} and D_{Na}, respectively) is shown in the Supporting Information **Figure S**5. Since π and F are both constants, and φ and D are also constants for a specific metal at the fixed temperature, the limit of the areal capacity, $C_{A\,lim}$ is then inversely proportional to the applied current density, I_D according to **Equation** (5). **Figure 3**a exhibits their relation at different temperatures for

both ASSLBs and ASSNBs. Apparently, at a defined temperature and I_D, the $C_{A\,lim}$ of ASSNBs is much higher than that of ASSLBs. As an example, the $C_{A,lim}$ is 0.6 mAh cm^{-2} for ASSLBs at 1.0 mA cm^{-2} and 25 °C, while the $C_{A,lim}$ is 21 mAh cm^{-2} for ASSNBs at the same I_D and temperature due to the difference between D_{Li} and D_{Na}, which are 5.1 × 10^{-11} and 5.4 × 10^{-9} cm^2 s^{-1} at 25°C, respectively (Supporting Information **Figure S**5). In principle, a higher D_{Na} ensures the fast refilling of the metal-voids created by current and results in a higher $C_{A,lim}$. The above calculation is based on an "ideal" solid electrolyte, also with flawless interface with Na-metal, which is independent of any practical electrolyte and practical interfaces. To investigate the practical limit of areal capacity, constant direct-current (DC) polarization tests were applied to Na/NSZP/Na symmetric ASSNBs, as shown in **Figure 3**b. As predicted above, the contact loss between Na metal and NZSP happens after a certain time of DC polarization applying constant current, indicated by the steep increase of the voltage of the symmetric ASSNBs. The sudden increase of voltage at the end of the DC polarization experiment could also be understood from **Equation** (3). The time for the metal to deplete from the solid electrolyte is proportional to the inverse of the effective current density to the power of 2. This means in practice that when point contact starts to form as mentioned above, the local current density is much higher than the apparent current density, the contact between the metal electrode and solid electrolyte will then decrease much faster, resulting in even higher local current density. Nevertheless, the inflexion point in the curves of **Figure 3**b represent the practical critical time. The practical limit of areal capacity for these ASSNBs is then also known and shown in **Figure 3**c. For comparison, the calculated $C_{A,lim}$ for ASSNBs are also shown, as well as the calculated and practical $C_{A,lim}$ for ASSLBs (practical $C_{A,lim}$ for ASSLBs were achieved by Li / $Li_7La_3Zr_2O_{12}$ / Li symmetric cells prepared and tested similar to the cells in present study). In general, the experimental areal capacity of ASSNBs is always lower than the

calculated ones. On one hand, the real interface between metal and ceramic contains impurities and is less perfect as assumed in the mathematical model. On the other hand, the actual processes on the metal / ceramic interface are more complicated than the assumptions in the present work. Except for the diffusion process influenced by the self-diffusion coefficient and expressed by Fick's second law, other mechanisms like additional vacancy formation and accumulation, pore formation and growth, etc., which are mainly controlled by the surface energy of both ceramic and metal, and interface energy of ceramic / metal interface [30], also potentially effect the actual interface between metal and ceramic during operation. The present work only offers the maximum critical time under extreme conditions. For ASSNBs at 1.0 mA cm^{-1} and 25 °C, the theoretical and experimental value of the symmetric cell have a moderate difference of between 21 mAh cm^{-2} and 18 mAh cm^{-2}, respectively (**Figure 3**c), indicating a nearly clean interface between the NZSP and Na metal. It also must be mentioned that not only the calculated $C_{A,lim}$, but also the practical $C_{A,lim}$of ASSNBs in this work are much higher than the calculated $C_{A,lim}$ of ASSLBs (**Figure 3**c), which presents the maximum of the areal capacity that ASSLBs can reach in practice, indicating the superiority of ASSNBs compared to ASSLBs in terms of dendrite-tolerance. Although there might be other influences as mentioned above, the difference of the self-diffusion coefficient between Na and Li should be one of the major reasons.

Figure 3d schematically explain the practical DC-polarization behavior for ASSLBs and ASSNBs. In the local area with surface roughness, surface impurities, grain boundaries etc., lower conductivity is expected compared to the transport directly in contact with NZSP grains, and resulting in lower local current density. This will result in the formation of voids on the spots with higher conductivity because the Na oxidation is faster on these surfaces. The formation of the voids also results in point contacts between the metal electrode and ceramic

electrolyte, while the point contacts are commonly regarded as the reason for dendrite formation because of the very high local current and electrochemical potential in the point-contact area [7, 11, 13, 15-17]. This is also the reason why an extra pressure of 3 – 7 MPa during operation of ASSLBs can increase the dendrite-tolerance [16]: The formation of the voids can be weakened under pressure because of the softness of Li-metal. Nevertheless, in the case of ASSNBs, the formation of voids and point contacts is dynamically slower compared to those of ASSLBs because of the higher self-diffusion coefficient. Even without extra pressure, the ASSNBs in the present study show similar performance to ASSLBs with applied pressure of several MPa, indicating their higher dendrite-tolerance. As alternative technology, Krauskopf et al. proposed very recently the use of alloying Mg with Li, which increasing the self-diffusion coefficient by the factor of three times (compared to pure Li), and the dendrite tolerance also increased accordingly [31]. In this study, Na naturally has a self-diffusion coefficient 2 orders of magnitude higher than Li.

3.3 Electrochemical behaviors of SSNBs full-cells

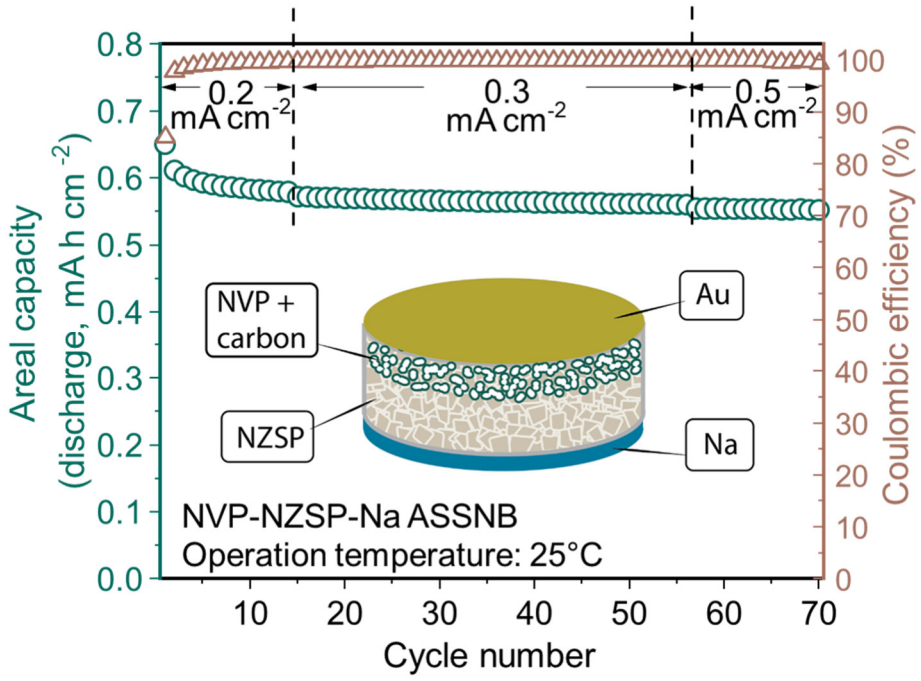

Figure 4. Discharge capacity and Coulombic efficiency at different levels of current density of a typical ASSNB full cell depending on the cycle numbers.

In the present study, we also prepared full battery cells to verify the realization of high performance cells. The ultimate goal of the current research is to develop ASSNBs which can be operated at high current density and high areal capacity without dendrite formation. For full cells, the preparation of the anodes is as simple as for symmetric cells, where sodium sheets were directly mechanically stuck to the NZSP ceramic. While the preparation of the cathode is based on an infiltration technique, where the cathode active material, $Na_3V_2(PO_4)_3$ (NVP, carbon coated) was produced on the pore-walls of NZSP backbones in the form of a nano-layer. All the interfaces in the full cells are pure inorganic (ceramic-ceramic or metal-ceramic) without liquid or polymer phase involved. The sketch of the full-cell design is shown in **Figure 4** and reported with more details elsewhere [20]. The outer appearance and the microstructure of a

typical sample is shown in the Supporting Information **Figure S**6. Such cathode design provides effective pathways for both electronic and ionic transfer, and minimizes the stress caused by volume change of cathode active materials. Typical cycling performance of the cells is shown in **Figure 4**, with a mass loading of active cathode materials (NVP) of 6.2 mg cm^{-2}, and the thickness of the cathode layer is 1 mm. After 3 cycles of stabilization, the cell has a discharge areal capacity of 0.60mAh cm^{-2} (specific capacity of 97 mAh g^{-1}) with a Coulombic efficiency of 98.5% (which gradually increases to 99.5% by the 10^{th} cycle). After operating at the current densities of 0.2, 0.3 and 0.5 mA cm^{-2} (0.3 C to 0.7 C, calculated based on NVP's theoretical capacity) for a total of 70 cycles at 25 °C, the areal capacity still remains 0.55 mAh cm^{-2} with a Coulombic efficiency of 99.5%, indicating the stability of the cell. Very recently, Tsai et al. [32] and Ma et al. [33] reviewed more than 30 representative ASSLBs and ASSNBs operating in the temperature range of 20 – 200 °C, the current density applied in the present study is one of the highest. The dendrite-free anode in the full cell is of course part of the reason for the high current density of the full cell. Moreover, judging from the behavior of symmetric cells in **Figure 1**, the current density of 0.5mA cm^{-2} in the full cell is still not the limit for the anode side. However, with higher current density (0.75 mA cm^{-2}, or 1 C), the cathode shows initial instability (Supporting Information **Figure S**7). The areal capacity and the operating current densities are higher than that published for most ASSLBs and ASSNBs. Actually, if only the areal capacity achieved at room temperature is considered, no ASSLBs or ASSNBs reached the level as in the present study [20, 31]. However, the performance is still far away from the expected criterion for practical application (≥ 3 mAh cm^{-2}) [10]. Further optimizations should especially be concentrated on the cathode side.

3.4 Discussions

In general, the dendrite formation is regarded as a result of point contacts between the metal anode and ceramic electrolyte [7, 11, 13, 15-17]. The point contacts start from the formation of voids in the metal anode near the metal/ceramic interface, which originates from the insufficient metal self-diffusion. The present approach cannot directly answer the question of when the dendrite will form. However, it gives the evaluation of the upper limit of the concerned areal capacity to avoid the dendrite formation, i.e. at a certain I_D, a critical operation time (i.e. critical areal capacity, the $C_{A\,lim}$) exists for ASSNB operation. Dendrite formation definitely occurs before the critical operation time (i.e. smaller than the $C_{A\,lim}$) due to the imperfections of the real interface. If the quality of the interface is improved, the occurrence of dendrite should be closer to the theoretical level. This also explains the influence of time as a parameter in CCD measurements (**Figure 1**b). When the step time in CCD measurements increases and approaches the critical operation time, the chance of dendrite occurrence also becomes higher, and results in lower I_D in the CCD measurements accordingly. This is the reason why intervals of 5 minutes result in a CCD as high as 9 mA cm^{-2}, while when the intervals are 30 minutes, the CCD decreases to about 3 mA cm^{-2} (**Figure 1**b and **Figure S3**b).

Since Li and Na metals show a significant difference in the intrinsic property of the metal self-diffusion coefficient (5.1×10^{-11} and 5.4×10^{-9} cm^2 s^{-1} at 25 °C, respectively, **Figure S**5), according to **Equation** (5) and **Figure 3**a, ASSNBs have certain advantages in dendrite tolerance compared to ASSLBs. Of course, although the calculated $C_{A\,lim}$ is only 0.6 mAh cm^{-2} for ASSLBs at 1.0 mA cm^{-2} and 25 °C, this does not mean that ASSLBs cannot reach the expected criteria of areal capacity ≥ 3 mAh cm^{-2} at current densities of ≥ 1 mA cm^{-2} [10]. The calculation is based on five assumptions (see section 3.2), which can be modified or changed. As an example, Hitz et al. [26] applied a three-dimensional anode structure instead of directly attaching metal to the solid-state electrolyte as in this study, where Li metal was deposited on

the porous scaffold of the Li-ion conductor as an anode layer, in which the metal-ceramic contact area is 40 times larger than the interface area between the flat anode and the electrolyte layers, resulting in an "apparent areal capacity" of 7.5mAh cm^{-2} at room temperature for the cell. Kasemchainan et al. [16] applied a pressure of 3 MPa during ASSLB operation, and achieved an areal capacity of 1.0 mAh cm^{-2} at 1.0 mA cm^{-2} and room temperature. There is also a simple way to satisfy the criteria by increasing the operation temperature: at 1.0 mA cm^{-1} and 50 °C, the $C_{A\ lim}$ of an ASSLB is 3.2 mAh cm^{-2} (see **Figure 3**a). For ASSNBs, expected criteria have been achieved with symmetric cells even without the above optimizations, but full cells need to be further improved. Besides, ASSNBs exhibit another advantage over ASSLBs: the yield strength of Na metal is smaller than that of Li metal (Na is softer than Li and hence easier to deform). When pressure has to be applied to compensate the insufficient transport due to the limiting metal self-diffusion, ASSNBs need lower pressure compared to ASSLBs, which is also important for practical application. Moreover, the possibility of using aluminum rather than copper as the current collector may result in lighter and cheaper full cells for ASSNBs compared to ASSLBs because Li metal will alloy with aluminum [2].

4. Conclusions

In conclusion, a low interface resistance of 1.7 Ω cm^2 between Na and NZSP is obtained at 25 °C. Na/NZSP/Na symmetric ASSNBs have a high CCD of 9 mA cm^{-2} at 25 °C, which decreases with increasing step-time. The ASSNBs can be operated at 1.0 mA cm^{-2} and 5 mAh cm^{-2} per half cycle at 25 °C, which is beyond the expected criterion of ASSLBs and ASSNBs and comparable with the-state-of-the-art lithium batteries using liquid or polymer electrolytes.. The high self-diffusion coefficient of Na metal results in the formation of fewer voids on the

interface between metal/solid electrolytes, suppresses the point contact and thus increases the dendrite tolerance. Based on the developed results of the ASSNB symmetric cells, full cells of NVP-C-NZSP/NZSP/Na also show stable cycling performance at an areal capacity of 0.6mAh cm^{-2} and a current density up to 0.5 mA cm^{-2}.

Acknowledgements

The authors thank Dr. D. Sebold (IEK-1) and Dr. D. Grüner (IEK-2) for SEM investigations. Partial financial support from China Scholarship Council (CSC) (file no. 201606210131) is acknowledged. Dr. Y. Ling gratefully acknowledges the financial support from the Humboldt foundation during his research stay at IEK-1.

Appendix A. Supporting Information

Supporting information data associated with this article can be found in the online version at:

References

[1] B. Dunn, H. Kamath, J.-M. Tarascon, *Science,* 334 (2011) 928-935.
[2] D. Larcher, J.-M. Tarascon, *Nature Chem.,* 7 (2015) 19-29.
[3] Lithium Statistics and Information, U.S. Geological Survey, **2019**, https://minerals.usgs.gov/minerals/pubs/commodity/lithium/.
[4] N. Yabuuchi, K. Kubota, M. Dahbi, S. Komaba, *Chem. Rev.,* 114 (2014) 11636-1168.
[5] W.Hou, X. Guo, X. Shen, K. Amine, H. Yu, J. Lu, *Nano Energy,* 52 (2018) 279-291.
[6] Y. Zhao, K. R. Adair, X. Sun, *Energy Environ. Sci.,* 11 (2018) 2673-2695.
[7] L. Fan, S. Wei, S. Li, Q. Li, Y. Lu, *Adv. Energy Mater.,* 8 (2018) 1702657.
[8] C. Zhao, L. Liu, X. Qi, Y. Lu, F. Wu, J. Zhao, Y. Yu, Y.S. Hu, L. Chen, *Adv. Energy Mater.,* 8 (2018) 1703012.
[9] J. Janek, W.G. Zeier, *Nat. Energy,* 1 **(**2016) 16141.
[10] P. Albertus, S. Babinec, S. Litzelman, A. Newman, *Nat. Energy,* 3 (2018) 16-21.
[11] H. Wang, D. Yu, C. Kuang, L. Cheng, W. Li, X. Feng, Z. Zhang, X. Zhang, Y. Zhang, *Chem,* 5 (2019) 313–338.
[12] W. Zhou, Y. Li, S. Xin, J. B. Goodenough, *ACS Cent. Sci.,* 3 (2017) 52-57.

[13] C.-L. Tsai, V. Roddatis, C. V. Chandran, Q. Ma, S. Uhlenbruck, M. Bram, P. Heitjans, O. Guillon, *ACS Appl. Mater. Interfaces,* 8 (2016) 10617-10626.
[14] A. Sharafi, E. Kazyak, A. L. Davis, S. Yu, T. Thompson, D. J. Siegel, N. P. Dasgupta, J. Sakamoto, *Chem. Mater.,* 29 (2017) 7961-7968.
[15] T. Krauskopf, H. Hartmann, W.G. Zeier, J. Janek, *ACS Appl. Mater. Inter.,* 11 (2019) 14463-14477.
[16] J. Kasemchainan, S. Zekoll, D. S. Jolly, Z. Ning, G. O. Hartley, J. Marrow, P. G. Bruce, *Nat. Mater.,* 18 (2019) 1105–1111.
[17] M. J. Wang, R. Choudhury, J. Sakamoto, *Joule*, 3 (2019) 2165-2178.
[18] Q. Ma, C.-L. Tsai, X.-K. Wei, M. Heggen, F. Tietz, J. T. S. Irvine, *J. Mater. Chem. A,* 7 (2019) 7766–7776.
[19] Q. Ma, M. Guin, S. Naqash, C.-L. Tsai, F. Tietz, O. Guillon, *Chem. Mater.,* 28 (2016) 4821-4827.
[20] T. Lan, C.-L. Tsai, F. Tietz, X.-K. Wei, M.Heggen, R. E. Dunin-Borkowski, R.Wang, Y. Xiao, Q. Ma, O. Guillon, *Nano Energy,* 65 (2019) 104040.
[21] S. Song, H. M. Duong, A. M. Korsunsky, N. Hu, L. Lu, *Sci. Rep*., 6 (2016) 32330.
[22] Y. Ruan, F. Guo, J. Liu, S. Song, N. Jiang, B. Cheng, *Ceram. Inter.*, 45 (2019) 1770–1776.
[23] Y. Lu, J. A. Alonso, Q. Yi, L. Lu, Z. L. Wang, C. Sun, *Adv. Energy Mater.*, 9 (2019) 1901205.
[24] E. Matios, H. Wang, C. Wang, X. Hu, X. Lu, J. Luo, W. Li, *ACS Appl. Mater. Interfaces* 11 (2019) 5064-5072.
[25] M. S. Park, S. B. Ma, D. J. Lee, D. Im, S.-G. Doo, O. Yamamoto, *Sci. Rep.,* 4 (2014) srep03815.
[26] G. T. Hitz, D. W. McOwen, L. Zhang, Z. Ma, Z. Fu, Y. Wen, Y. Gong, J. Dai, T. R. Hamann, L. Hu, E. D. Wachsman, *Mater. Today*, 22 (2019) 50-57.
[27] N. J. Taylor, S. Stangeland-Molo, C. G. Haslam, A. Sharafi, T. Thompson, M. Wang, R. Garcia-Mendez, J. Sakamoto, *J. Power Sources,* 396 (2018) 314-318.
[28] R. Sudo, Y. Nakata, K. Ishiguro, M. Matsui, A. Hirano, Y. Takeda, O. Yamamoto, N. Imanishi, *Solid State Ionics,* 262 (2014) 151-154.
[29] F.G. Cottrell, *Z. Phys. Chem.,* 42 (1903) 385-431.
[30] M. Bobeth, M. Gutkin, W. Pompe, A. E. Romanov, *phys. stat. sol. (a)*, 165 (1998) 165-184.
[31] T. Krauskopf, B. Mogwitz, C. Rosenbach, W. G. Zeier, J. Janek, *Adv. Energy Mater.,* 9 (2019) 1902568.
[32] C.-L. Tsai, Q. Ma, C. Dellen, S. Lobe, F. Vondahlen, A. Windmüller, D. Grüner, H. Zheng, S. Uhlenbruck, M. Finsterbusch and et. al, *Sustain. Ener. Fuels*, 3 (2019) 280–291.
[33] Q. Ma, F. Tietz, *ChemElectroChem*, doi.org/10.1002/celc.202000164.